

# Towards construction of microscopic model for smart coating of a solid surface

O. Pizio  \*

Instituto de de Química, Universidad Nacional Autónoma de México, Circuito Exterior, 04510, Ciudad de México, México

Received April 17, 2024, in final form June 12, 2024

The density functional approach for classical associating fluids is used to explore the wetting phase diagrams for model systems consisting of water and graphite-like solid surfaces chemically modified by a small amount of grafted chain molecules. The water-like fluid model is adopted from the work of Clark et al. [Mol. Phys., **104**, 3561 (2006)]. It very well describes the bulk water vapor-liquid coexistence. Each chain molecule consists of tangentially bonded hard sphere segments. We focus on the investigation of the growth of water film on such complex substrates and exploration of the wetting behavior. For grafted monomers, the prewetting phase diagrams are similar to the diagrams for water on a non-modified solid surface. However, for grafted trimers and pentamers, a physically much richer behavior is observed and analyzed. Trends of the behavior of the wetting temperature and the prewetting critical temperature on the grafting density and water-segments attraction are discussed in detail.

**Key words:** *density functional theory, water model, density profiles, adsorption, wetting temperature*

## 1. Dedication and history lessons

The year 2024 has been marked by unfortunate, profoundly sad events for me. On March 26, my teacher Ihor Rafailovych Yukhnovskii passed away. He kindly, with much patience guided my education and growth during first two decades of my scientific career, starting from 1973 at the Department for Statistical Theory of Condensed Systems of the Institute for Theoretical Physics of the Academy of Sciences of the UkrSSR, till my departure to take a new job in Mexico in 1993. He tried to convert me into the follower of the “true faith” of his collective variables method, that I recall nowadays as a fascinating endeavour. The present manuscript is dedicated to the 100th anniversary of Prof. I. Yukhnovskii birth and as a modest tribute due to his important contributions to the theory of soft condensed matter.

This story started at pre-internet times and simultaneously with computer simulations revolution that influenced the way of thinking of many theoreticians including I. Yukhnovskii. One of the lines of research initiated by Prof. I. Yukhnovskii was to explore the classical ion-molecular fluids under the influence of external field. In fact, this area represents one of the most important fundamental problems of the microscopic liquid state theory that is related to various applications and technological developments.

The first works of Yukhnovskii and collaborators, published in 1959, concerned the formulation of the density profiles in terms of the screened potentials of long-range electrostatic interactions and of the free energy of the model electrolyte of point charges as the Mayer-type cluster series [1] within the collective variables method. The short-range interactions were taken into account by functional differentiation and contribute as the Boltzmann factors, in, e.g., the virial coefficients of the free energy. On the other hand, the screening potential of electrostatic interactions was obtained as the solution of the convolution type integral equation coming from the approximation for the transition Jacobian from the Cartesian coordinates to the collective variables.

\*Corresponding author: [opizio@gmail.com](mailto:opizio@gmail.com).

This pioneering work appeared at the same period of time as the Percus and Yevick integral equation for a hard sphere fluid model [2] and much earlier than the statistical mechanical procedure proposed by Henderson, Abraham and Barker [3] to describe simple fluids in contact with hard solid wall. This kind of approach was extended to systems with Coulomb inter-particle interaction besides hard sphere repulsive forces, by Blum et al. [4, 5] almost immediately at the level of the mean spherical approximation.

By contrast, Yukhnovskii and his younger co-workers persuaded the development of the collective variable method to inhomogeneous fluids with long-range electrostatic interactions considering electrolyte solution type models and assuming the presence of a sharp uncharged boundary and the dielectric discontinuity in the system [6–9].

At the early seventies of the last century (around 1970–1972), I. Yukhnovskii reconsidered the developments from the integral equations method for simple fluids with dominating short-range repulsive interaction, principally under the influence of his long-term co-worker Prof. M. Holovko. As a result, the reference system reformulation of the transition Jacobian to collective variables was developed by Yukhnovskii. Within this methodological procedure, the screening potentials follow from the Ornstein-Zernike type integral equations both for homogeneous and non-homogeneous ion-molecular fluids. Next, the expressions for the free energy and pair distribution functions are obtained straightforwardly (as in the original version of the collective variables method). These series were termed as the optimized cluster expansions. One example of the application of this procedure for the ion-dipole model electrolyte by using the screening potentials from the solution of the mean spherical approximation is given in [10].

A comprehensive account of the versions of the collective variables method together with the integral equations theories for various model fluids with the emphasis on ion-molecular mixtures is given in the extraordinarily important monograph by Yukhnovskii and Holovko [11]. This book provides a profound analysis of the relations between different methods and regarding the limits of their applicability. Moreover, the book outlined necessary developments that in fact inspired various posterior works. A brief account of the results concerning the screening potential for inhomogeneous ion-molecular model fluids of point-like particles is also available in [12, 13].

In 1991 Ukraine regained its independence. I. R. Yukhnovskii, as a prominent scientist and one of intellectual leaders of the nation, interrupted his scientific activities becoming involved in the top governmental bodies and the parliament of the new state. The ensuing efforts in the construction of the theory of inhomogeneous fluids, mixtures and electrolyte solutions were undertaken by the academic stuff grown in the Department for Theory of Solutions of the ICMP (Institute for Condensed Matter Physics of the National Academy of Sciences of Ukraine) guided by Prof. M. Holovko at that time.

Principal efforts in the area of research were undertaken in the extensions of the available methods to deal with strong inter-particle attraction or, in other words, to take into account the chemical association of species. Specifically, theoretical foundations of the approach by Wertheim in terms of multi-density thermodynamic perturbation theory and integral equations of the Ornstein-Zernike type for differently associated species in the bulk, homogeneous fluids served for this purpose. To be brief and closer to the objective of the present manuscript, I would like to refer to some first studies concerning inhomogeneous associating fluids [14–16]. In contrast to these, early studies using integral equations methodology, the ensuing efforts from this laboratory were performed within density functional approaches for associating fluids [17]. It is worth mentioning that general aspects of the relation between collective variables and density functional approaches were elucidated some time ago [18].

Concerning our applications of this technique to systems with non-electrostatic inter-particle interactions, we explored the two-site and four-site fluid models with site-site chemical association, besides Lennard-Jones inter-particle attraction, in contact with various solid surfaces and in pores of different geometry [19–22]. Our interest to revisit all these findings and explore novel systems, in part, had arisen due to a successful parametrization of the four-site water model with square well non-associative attraction, in the laboratory of G. Jackson [23]. The model and method permitted to obtain novel insights into adsorption and phase behavior of water in nanoscopic slit-like pores [24, 25]. More recently, we considered the effects of fluid-solid interaction strength on the wetting of graphite-like solids by water [26]. In that work, the temperature dependence of the contact angle for water on different substrates was obtained from the Young equation besides the exploration of adsorption isotherms. Trends of behavior of the contact angle permitted to make estimates for the wetting temperature of water as well. With this knowledge, we have attempted to study the phase behavior, adsorption, wetting temperature and contact angle for several

systems that involve more complex substrates. Namely, we considered the behavior of water in contact with graphite-like solid surfaces that are chemically modified by grafting of chain molecules and their mixtures [27, 28]. As a by-product, the contact angle of water model on solids with grafted monomer species was explored as well [29]. Unfortunately, on June 24 of 2024, my very close friend, Stefan Sokolowski, with whom we permanently worked together during three decades, since 1994, suddenly passed away [30]. All theoretical background used to elaborate the present manuscript is the product of our common efforts. The principal scientific objective of this manuscript and formal introduction are given in the next section.

## 2. Introduction

Chemically modified solid substrates are common objects in contemporary surface science. They are intentionally designed to produce surfaces with desired specific properties or functionalities. Grafting chain particles (oligomers and/or polymers) is one of the powerful methods to yield functionalized surfaces that have an enormous area of applications. One kind of systems resulting from such a procedure is termed as polymer brushes [31]. As an opposite extreme, a rather small molecule can be used for surface functionalization [32–34] with quite different purposes. One example of frequently used modifiers of silica-based surfaces is 3-Aminopropyltriethoxysilane (APTES) molecule [33, 34]. It can be viewed (in coarse grained representation) as a molecule composed of four segments. APTES can covalently attached to the silica surface through the formation of siloxane bonds, whereas its amine group extends away from the substrate. This type of modified solid surfaces, in general terms, is used for selective adsorption of undesirable species from aqueous media. However, adsorption of the dominant component, i.e., of water solvent, upon the changes of the conditions of the experiment or process, should be known prior to the study of aqueous solutions.

Trends of behavior of adsorption can be interpreted in terms of wetting. Majority of experimental and theoretical studies in the literature concern the wetting of water by smooth homogeneous solid substrates. The influence of substrate heterogeneity, at macro or mesoscopic scale, on the adsorption and wetting has been considered in several publications as well. From the previous analyses, it is expected that the wetting properties of modified surfaces due to grafted molecules are different, in comparison with bare (or non-modified solids) [35–37].

Usually, the wetting transition, between non-wetting and wetting behavior, is elucidated by two methods. One of them is based on the measurement of the contact angle,  $\theta$ . The wetting transition takes place when  $\theta$  drops from a non-zero value to zero. The characteristic temperature at which such a change occurs is the wetting temperature. On the other hand, another experimental method to determine the wetting temperature relies on the evaluation of the adsorption isotherms for gas densities up to the density of the bulk saturated vapor at different temperatures. Then, one can recover the line of the first-order prewetting transition that starts at the wetting temperature and ends up at the prewetting critical temperature for, e.g., strongly attractive substrates. It is important to mention that the method based on adsorption isotherms permitted to obtain experimental wetting temperature and the prewetting transition temperature for  $^4\text{He}$  on cesium for the first time [38]. Both these methods formally can be implemented within the relevant theoretical procedures. One can evaluate the quality of modelling the system with respect to the indicators of its interfacial behavior.

In fact this task is not straightforward. The wetting behavior follows from an interplay between fluid-fluid and fluid-solid interaction, besides the interactions involving segments of grafted molecules with fluid species and with solid surface. Finally, the interaction between segments of different grafted molecules matter as well. Consequently, certain assumptions or simplifications are inevitable within theoretical modelling. If the grafted molecules are long chains, mimicking polymer species, and if one restricts to the brush regime, the interactions of fluid species and of exposed segments with solid substrate can be neglected. On the other hand, if the grafted species are short, one should find arguments to choose the values of parameters for the entire set of interactions.

Theoretical approaches to the study of adsorption of fluids on solids modified with grafted chain molecules are usually based on different versions of density functional (DF) methods [39–44]. Our approach, as in the previous works from this laboratory, is based on the theory of adsorption of a mixture

of chain molecules, developed by Yu and Wu [45]. The theory is successful in describing the wetting and layering transition [46, 47], as well as phase transitions in fluids confined to nanoscopic slit-like pores with modified walls [48, 49].

In our recent work [26] we investigated a prewetting transition for water adsorbed on graphite-like substrates using the density functional approach for classical associating fluids. Water-water interactions were modelled according to the SAFT approach [50]. The fluid-solid interaction, however, is assumed to have a 10-4-3 Lennard-Jones type potential form [51]. The interaction energy of the latter potential is considered to be a free parameter while the wetting and the prewetting critical temperatures as well as the prewetting phase diagrams are evaluated for different fluid-solid attractions. Theoretical findings are in agreement with the experimental results [52] as well as with data from computer simulations [53–56]. In spite of less sophisticated modelling of the system within the density functional approaches in comparison with computer simulations, theoretical calculations provide a rather comprehensive description of the wetting phenomena. Theoretical calculations are computationally less expensive and faster than computer simulations performed with the same goal. Therefore, the density functional approach provides a convenient tool to study the adsorption and phase behavior of associating fluids on the solids modified with tethered chain molecules.

The principal aim of this paper is to study the wetting behavior of water-like species on graphite-like surfaces modified by short tethered chain molecules. Then, the phase diagrams can be compared with their counterparts for non-modified surfaces [26]. The present work is a continuation of our previous studies of adsorption and wetting of surfaces with tethered chains [46, 47]. We restrict ourselves to the study of the models of grafted species (monomers, trimers and pentamers) built of hard-sphere segments. However, the segments of grafted species may attract water molecules. The principal issues of the study lie on the influence of the grafting density and the number of segments of the grafted molecules on the prewetting transition. A comparison of adsorption trends of water and the wetting behavior for grafted and ungrafted models is performed.

### 3. Model

We study a model for adsorption of water on graphite-type solid modified with end-grafted chain molecules. The fluid particles and grafted molecules are considered as a mixture of species put in contact with a wall. The grafted molecules are the chains built of  $M$  tangentially bonded spherical hard segments of diameter  $\sigma_s$ . The connectivity of segments belonging to a given molecule is provided by imposing the bonding potential,  $V_B$  [45],

$$\exp[-\beta V_B(\mathbf{R})] = \prod_{i=1}^{M-1} \delta(|\mathbf{r}_{i+1} - \mathbf{r}_i| - \sigma_s) / 4\pi\sigma_s^2, \quad (3.1)$$

where  $\mathbf{R} \equiv (\mathbf{r}_1, \mathbf{r}_2, \dots, \mathbf{r}_M)$  is the vector specifying the positions of segments,  $\delta$  is the Dirac function, and  $\beta = 1/k_B T$ .

The first segment of each chain molecule is irreversibly bonded to the substrate by the potential, see, e.g., [48, 49, 57, 58],

$$\exp[-\beta v_{s_1}(z)] = C \delta(z - \sigma_s/2), \quad (3.2)$$

where  $z$  is a distance from the surface and  $C$  is a constant. Thus, the model implies that the surface-binding segments are at a fixed distance from the surface along  $z$ -axis although they can slide within the  $xy$ -plane. The solid surface is an impenetrable hard wall for all other segments  $i = 2, 3, \dots, M$ ,

$$v_{s_i}(z) = \begin{cases} \infty, & z \leq \sigma_s/2, \\ 0, & z > \sigma_s/2. \end{cases} \quad (3.3)$$

The interactions between water molecules are described by the model from [59, 60] parameterized by Clark et al. [23]. As the rationale for the choice of the interaction potential was given in [23], we would like to recall solely a few issues. Each fluid molecule possesses four associative sites denoted as A, B,

C, and D, inscribed into a spherical core. The set of all the sites is denoted by  $\Gamma$ . The pair interlocutor potential between molecules 1 and 2 depends on the center-to-center distance and orientations,

$$u(r_{12}) = u_{\text{ff}}(r_{12}) + \sum_{\alpha \in \Gamma} \sum_{\beta \in \Gamma} u_{\alpha\beta}(\mathbf{r}_{\alpha\beta}), \quad (3.4)$$

where  $\mathbf{r}_{\alpha\beta} = \mathbf{r}_{12} + \mathbf{d}_{\alpha}(\omega_1) - \mathbf{d}_{\beta}(\omega_2)$  is the vector connecting site  $\alpha$  on molecule 1 with site  $\beta$  on molecule 2,  $r_{12} = |\mathbf{r}_{12}|$  is the distance between centers of molecules 1 and 2,  $\omega_i$  is the orientation of the molecule  $i$ ,  $\mathbf{d}_{\alpha}$  is the vector from the molecular center to the site  $\alpha$ , see, e.g., figure 1 of [59] for better visualization. Each of the off-center attraction sites is located at a distance  $d_s$  from the particles' center,  $d_s = |\mathbf{d}_{\alpha}|$  ( $\alpha = A, B, C, D$ ).

Only the site-site association AC, BC, AD, and BD is allowed and all site-site association energies are assumed equal. The interaction between sites is given as

$$u_{\alpha\beta}(\mathbf{r}_{\alpha\beta}) = \begin{cases} -\varepsilon_{\text{as}}, & \text{if } 0 < |\mathbf{r}_{\alpha\beta}| \leq r_c, \\ 0, & \text{if } |\mathbf{r}_{\alpha\beta}| > r_c, \end{cases} \quad (3.5)$$

where  $\varepsilon_{\text{as}}$  is the depth of the association energy well and  $r_c$  is the cut-off of the associative interaction.

The non-associative part of the pair potential,  $u_{\text{ff}}(r)$ , is given as

$$u_{\text{ff}}(r) = u_{\text{hs,ff}}(r) + u_{\text{att,ff}}(r), \quad (3.6)$$

where  $u_{\text{hs,ff}}(r)$  and  $u_{\text{att,ff}}(r)$  are the hard-sphere (hs) and attractive (att) pair interaction potential, respectively. The hs term is,

$$u_{\text{hs,ff}}(r) = \begin{cases} \infty, & \text{if } r < \sigma, \\ 0, & \text{if } r \geq \sigma, \end{cases} \quad (3.7)$$

where  $\sigma$  is the hs diameter. The attractive interaction is described by the square-well potential,

$$u_{\text{att,ff}}(r) = \begin{cases} 0, & \text{if } r < \sigma, \\ -\varepsilon, & \text{if } \sigma \leq r < \lambda\sigma, \\ 0, & \text{if } r \geq \lambda\sigma, \end{cases} \quad (3.8)$$

where  $\varepsilon$  and  $\lambda$  are the depth and the range of the non-associative attraction potential, respectively.

According to the model design [23], four sets of parameters of the potentials from equation (3.5) and equation (3.8) were proposed. They are denoted as W1, W2, W3, and W4 models. The W1 model slightly better reproduces the bulk phase diagram and the temperature dependence of the surface tension of water than the W2, W3 and W4 models, see figure 2 of [47] and data resorted in [23, 26] for these properties. The parameters of the W1 model are given here in table 1 for the convenience of the reader.

**Table 1.** The parameters of the W1 water-water model potential from [23].

Model	$\sigma$ (nm)	$(\varepsilon/k)$ (K)	$\lambda$	$r_c$ (nm)	$(\varepsilon_{\text{as}}/k)$ (K)	$d_s/\sigma$
W1	0.303420	250.000	1.78890	0.210822	1400.00	0.25

The interaction of water molecules with carbonaceous solids is described by the potential developed by Steele [51]. It reads,

$$v_{\text{sf}}(z) = 2\pi\rho_g\varepsilon_{\text{sf}}\sigma_{\text{sf}}^2\Delta \left[ \frac{2}{5} \left( \frac{\sigma_{\text{sf}}}{z} \right)^{10} - \left( \frac{\sigma_{\text{sf}}}{z} \right)^4 - \frac{\sigma_{\text{sf}}^4}{3\Delta(z + 0.61\Delta)^3} \right], \quad (3.9)$$

where  $\varepsilon_{\text{sf}}$ ,  $\sigma_{\text{sf}}$  are the energy and the distance parameters, respectively;  $\Delta$  is the interlayer spacing of the graphite planes,  $\Delta = 0.335$  nm and  $\rho_g$  is the density of graphite,  $\rho_g = 114$  nm<sup>-3</sup>. To calculate the value of  $\sigma_{\text{sf}}$  we applied Lorentz additivity rule,  $\sigma_{\text{sf}} = (\sigma_g + \sigma)/2$ , where  $\sigma_g = 0.34$  nm is the diameter of carbon atoms in graphite. Some aspects of the applicability of equation (3.9) are discussed in [51, 56]. On the

other hand, recently we showed that this potential can be successfully applied to describe the temperature dependence of the contact angle of water on graphite-like solids [26].

The interaction of water particles with each segment of grafted molecules is assumed in the form,  $u_{fc}(r) = u_{hs,fc}(r) + u_{att,fc}(r)$ . It is the same as for non-associative water-water interaction. In the hard sphere term, we choose  $\sigma_{fc} = \sigma_s = \sigma$  for simplicity. The attractive contribution is taken in the square-well form, similarly to equation (3.8), although with the parameters  $\lambda_{fc}$  and  $\varepsilon_{fc}$ . A reasonable choice of  $\lambda_{fc}$  and  $\varepsilon_{fc}$  is not straightforward. It should be based on any kind of experimental information that we lack at present. Finally, we assumed that the interaction between segments of different grafted chains is of hard sphere type with the parameter  $\sigma_s$ .

The grafting density of chain molecules is  $r_c = N_s/A$ ,  $N_s$  is the number of grafted molecules and  $A$  is the surface area. The system under study is considered in equilibrium with the reservoir containing water molecules only. The bulk density and the chemical potential of water are denoted as  $\rho_b$  and  $\mu$ , respectively.

## 4. Theory: density functional approach

We use the density functional approach based on the theory originally developed by Yu and Wu [45]. This approach has been already used to describe systems involving grafted layers [26, 48, 49, 57, 58]. The free-energy functional is constructed in the perturbation manner, i.e., it is the sum of the contributions arising from different interactions in the system,  $F = F_{id} + F_{hs} + F_c + F_{as} + F_{att}$ . The ideal part of the free energy,  $F_{id}$ , is known exactly [45]. The excess free energy due to hard-sphere interactions,  $F_{hs}$ , follows from the White Bear version of the Fundamental Measure Theory [61]. The chain connectivity contribution,  $F_c$ , as well as the contribution corresponding to the associative water-water interaction,  $F_{as}$ , result from the first-order perturbation theory of Wertheim [59–61].

Each of the above mentioned contributions is defined as a functional of the local density of fluid molecules,  $\rho(\mathbf{r})$ , and the densities of particular segments  $\rho_{s_i}(\mathbf{r})$ . These contributions were described in detail in [45, 61]. In addition, it is convenient to define the total segment density profile,

$$\rho_s(\mathbf{r}) = \sum_{i=1}^M \rho_{s_i}(\mathbf{r}). \quad (4.1)$$

The attractive free energy term results from the mean-field approximation,

$$F_{att} = \frac{1}{2} \int d\mathbf{r}_1 d\mathbf{r}_2 \rho(\mathbf{r}_1) \rho(\mathbf{r}_2) u_{att,ff}(|\mathbf{r}_1 - \mathbf{r}_2|) + \sum_{i=1}^M \int d\mathbf{r}_1 d\mathbf{r}_2 \rho(\mathbf{r}_1) \rho_{s_i}(\mathbf{r}_2) u_{att,fc}(|\mathbf{r}_1 - \mathbf{r}_2|), \quad (4.2)$$

where,  $u_{att,ff}(r)$  coincides with  $u_{att,fc}(r)$  introduced in the previous subsection. With the free energy constructed, the essence of the calculations is in the minimization of the thermodynamic potential. The grafted density is fixed by the constraint,

$$\int dz \rho_s(z) = R_c. \quad (4.3)$$

In the above equation we have taken into account that for one-dimensional external field as in equation (3.9), the local densities of segments and fluid molecules depend on the coordinate  $z$  only. If the constraint (4.3) is taken into account, the thermodynamic potential is given as,

$$\mathcal{Y} = F[\rho_s(z), \rho(z)] + \sum_{i=1}^M \int dz \rho_{s_i}(z) v_{s_i}(z) + \int dz \rho(z) [v_{sf}(z) - \mu]. \quad (4.4)$$

The Euler-Lagrange equations (cf. [26, 61]) that follow from the minimization of the thermodynamic

potential,

$$\frac{\delta \mathcal{Y}}{\delta \rho(z)} = 0, \quad (4.5)$$

$$\frac{\delta \mathcal{Y}}{\delta \rho_{s_i}(z)} = 0, \quad (4.6)$$

are solved numerically using Picard iteration algorithm. The solution yields the density profiles  $\rho(z)$ , and  $\rho_{s_i}(z)$  for  $i = 1, 2, \dots, M$  and the total profile of grafted species  $\rho_s(z)$  as a result.

The density profile  $\rho(z)$  determines the excess adsorption isotherm,

$$\Gamma_{\text{ex}} = \int dz [\rho(z) - \rho_b]. \quad (4.7)$$

The behavior of the grafted layer upon changing the external conditions can be described by using the first moment of the density profile  $\rho_s(z)$ . In the case of long grafted species in the brush regime, it is interpreted as a brush height,  $\langle h_c \rangle$ . It can be defined as [62, 63],

$$\langle h_c \rangle = 2 \int dz z \rho_s(z) / \int dz \rho_s(z). \quad (4.8)$$

Similarly to our recent study [26], the localization of the equilibrium transition along each isotherm relies on the calculations of the excess thermodynamic potential,  $\mathcal{Y} - \Omega_b$ , where  $\Omega_b$  denotes the grand canonical thermodynamic potential of the bulk fluid, along the increasing and decreasing chemical potential paths, starting the iterations from the density obtained at a previous value of the chemical potential.

Except otherwise stated, all the quantities are given in reduced units. The parameters characterizing water species,  $\sigma$  and  $\varepsilon$ , are chosen as the length and energy units. The reduced temperature then is  $T^* = k_B T / \varepsilon$ , the reduced distance is  $z^* = z / \sigma$ ,  $R_c^* = R_c \sigma^2$ ,  $\langle h_{\text{ch}}^* \rangle = \langle h_{\text{ch}} \rangle / \sigma$ , the reduced adsorption and reduced local density are  $\Gamma_{\text{ex}}^* = \Gamma_{\text{ex}} \sigma^2$ ,  $\rho^*(z) = \rho(z) \sigma^3$  (similarly,  $\rho_s^*(z) = \rho_s(z) \sigma^3$ ). In addition,  $\varepsilon_{\text{gs}}^* = 2\pi \rho_g \varepsilon_{\text{sf}} \sigma_{\text{sf}}^2 \Delta / \varepsilon$ , and  $\varepsilon_{\text{fc}}^* = \varepsilon_{\text{fc}} / \varepsilon$ .

For a given model of interaction between water molecules, the system is characterized by parameters. They are: the diameter of spherical segments, the number of segments  $M$ , the grafting density, and the parameters of the water-solid potential from equation (3.9). Principally, our calculations focused on the evaluation of the wetting properties, concern the changes of grafting density,  $R_c^*$ , for molecules composed of a different number of segments,  $M$ , and the interaction energy between water particles and segments of grafted molecules,  $\varepsilon_{\text{fc}}^*$ .

## 4.1. Results

Intuitively, one could expect that the influence of a small amount of grafted molecules on the prewetting phase behavior should be similar to the effect of decreasing the value of water-solid interaction strength,  $\varepsilon_{\text{gs}}^*$ . We would like to explore this issue more in detail.

To begin with, let us consider a set of results concerning the system of monomers,  $M = 1$ , grafted on a strongly adsorbing graphite-like solid with  $\varepsilon_{\text{gs}}^* = 9.5$ . Besides, we assume that the interaction between grafted monomers and water particles is of hard sphere type, i.e.,  $\varepsilon_{\text{fc}}^* = 0$ . If the grafted density changes from zero (bare substrate with a vanishing amount of grafted species) up to  $R_c^* = 0.7$ , the wetting temperature,  $T_w^*$ , changes from  $T^* = 1.76$  (bare substrate) to a high value,  $T^* \approx 2.63$ , quite close to the critical temperature of bulk water ( $T_c^* \approx 2.718$ ). This is illustrated in the chemical potential-temperature plane,  $\beta(\mu - \mu_0)$  ( $\mu_0$  is the chemical potential at bulk coexistence), figure 1a. The lines of the first-order prewetting transition, plotted in red with circles in each case, start from  $T_w^*$  and end up at a certain critical prewetting temperature  $T_{\text{cp}}^*$ , figure 1a. At  $T^* < T_w^*$ , water does not wet the surface. On the other hand, at  $T_{\text{cp}}^* < T^* < T_c^*$ , the adsorption isotherms are smooth. They tend to infinity upon approaching the bulk coexistence. Next, I performed calculations of the prewetting phase diagrams of non-grafted solid surfaces searching for the values of  $\varepsilon_{\text{gs}}^*$  that yield a similar value of the wetting temperature as for

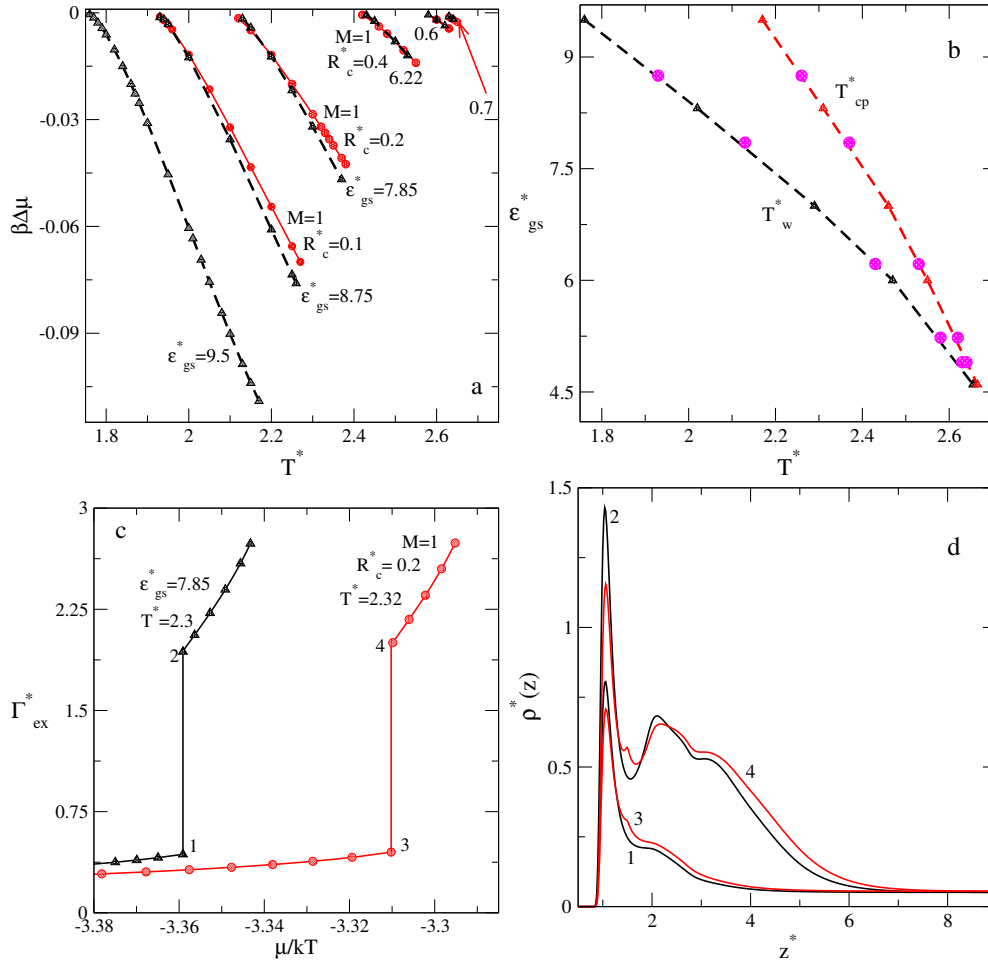


**Figure 1.** (Colour online) Panel a: The prewetting phase diagrams for water on graphite-like solid with different adsorbing strength ( $\epsilon_{gs}^* = 9.5, 8.75, 7.85, 6.22, 5.23$  and  $4.9$ , from the left to right, plotted as dashed lines with triangles). The last two numbers are omitted to make the figure less loaded. The diagrams for the model with grafted monomers at  $R_c^* = 0.1, 0.2, 0.4, 0.6$  and  $0.7$  are plotted as red solid lines with circles. Panel b: The characteristic temperatures,  $T_w^*$  and  $T_{cp}^*$  of the prewetting phase diagrams for two sets of models in  $\epsilon_{gs}^* - T^*$  plane. Dashed lines with triangles correspond to graphite-like solid with different adsorbing strength. Magenta circles indicate  $T_w^*$  and  $T_{cp}^*$  for the models with grafted monomers as in panel a. Panel c: Fragments of adsorption isotherms of two models illustrating the prewetting phase transition. Panel d: The density profiles of water species just before and after the prewetting transition at states numbered in panel c.

grafted systems. These results are plotted as black lines decorated by triangles. It can be seen that the lines describing two sets of phase diagrams nearly coincide, figure 1a. A small difference is observed, however, close to the critical temperature of prewetting. Still, if one constructs the curves for two characteristic temperatures,  $T_w^*$  and  $T_{cp}^*$ , in the  $\epsilon_{gs}^* - T^*$  plane, the magenta circles (corresponding to grafted systems with different  $R_c^*$ ) fit well on the curves describing the substrates of a different adsorbing strength without grafted monomers, figure 1b. From these results one can get an idea about the changes of wettability of the grafted systems using their non-grafted counterparts.

In addition, we observed that the jump of the excess adsorption upon the prewetting transition in two types of systems is quite similar even close to  $T_{cp}^*$ , figure 1c. The corresponding density profiles of water species, before and after the prewetting transition are shown in figure 1d. The presence of grafted monomers leads to a smaller values of the density profile in the region of the first maximum compared

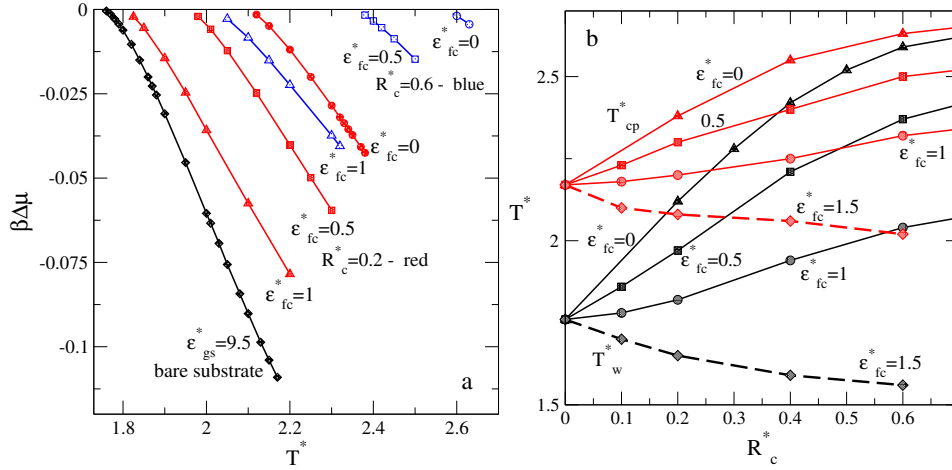


**Figure 2.** (Colour online) Panel a: Prewetting phase diagrams for water on a solid substrate with grafted monomers at  $R_c^* = 0.2$  (red lines with symbols) and  $0.6$  (blue lines with symbols). Circles, squares and triangles correspond to  $\epsilon_{fc}^* = 0, 0.5$  and  $1$ , respectively. Panel b: Evolution of the wetting temperature,  $T_w^*$ , and of the prewetting critical temperature,  $T_{cp}^*$ , on the grafting density,  $R_c^*$ , of monomers.

to the bare substrate. This tendency is less pronounced in the vapor phase (prior to the prewetting transition). By contrast, after the transition, the difference of height of the profiles is quite big. Thus, the fluid molecules are “expelled” from the vicinity of the substrate surface, presumably because the grafted monomers play the role of obstacles. Moreover, if the grafted monomers are present, the density profile exhibits a peculiarity at  $z \approx 1.5$ . In summary, augmenting grafting density of monomers,  $R_c^*$ , makes the functionalized substrate less and less hydrophilic and the equivalency with the decreasing value of  $\epsilon_{gs}^*$  can be well established. This conclusion is valid for the entire interval of  $R_c^*$ , i.e., up to two-dimensional packing fraction that yields a wetting temperature approaching the bulk critical temperature.

All the results presented in figure 1 were obtained assuming the hard-sphere type interaction between grafted monomers and water molecules,  $\epsilon_{fc}^* = 0$ . If the grafted monomers attract water species, the balance of repulsive and attractive forces changes. Consequently, the prewetting phase diagrams change. It is difficult to choose the values for the parameter  $\epsilon_{fc}^*$  appropriately without supporting the experimental evidence to intend reasonable parametrization. We have chosen  $\lambda_{fc} = 1.5\sigma$  fixed, and consider the augmenting values for  $\epsilon_{fc}^*$ . One can intuitively expect that the grafted layers of short molecules may quantitatively change the trends of behavior of the wetting properties rather than yield qualitative changes.

Two examples illustrating the changes of the prewetting phase diagram, for  $R_c^* = 0.2$  and  $0.6$ , are shown in figure 2a. Apparently, at a value of  $\epsilon_{fc}^*$  higher than shown for  $R_c^* = 0.2$ , one can obtain the wetting temperature even lower, compared to the bare substrate with  $\epsilon_{gs}^* = 9.5$ . The entire dependence of the wetting temperature,  $T_w^*$ , and of the prewetting critical temperature,  $T_{cp}^*$ , on the grafting density,  $R_c^*$ , with the parameters under study, is shown in figure 2b. Both dependencies,  $T_w^*(R_c^*)$  and  $T_{cp}^*(R_c^*)$  are non-linear. Moreover, at  $\epsilon_{fc}^* = 1.5$ , the wetting temperature decreases upon increasing  $R_c^*$ , indicating that the grafted surface becomes more hydrophilic than the bare substrate, if water molecules strongly surround or cover the attractive monomer obstacles. It seems that at this value for  $\epsilon_{fc}^* = 1.5$ , the system is still above the possible triple point temperature. One should have in mind, that the water model in question has been parametrized for temperatures above the triple point temperature. Therefore, the application of theoretical construction may be questionable at lower temperatures.

A very similar set of calculations were performed for the systems with grafted chain particles made of three monomers ( $M = 3$ ). The first series of calculations were performed for the systems in the absence of segment-water attraction,  $\epsilon_{fc}^* = 0$ . These short chains were grafted on a strongly adsorbing substrate with  $\epsilon_{gs}^* = 9.5$ . If the grafting density increases from zero up to  $R_c^* = 0.1$ , the wetting temperature changes from its value for a pure substrate,  $T_w^* = 1.76$ , to  $T_w^* = 2.64$ , quite close to the bulk water critical temperature, figure 3a.

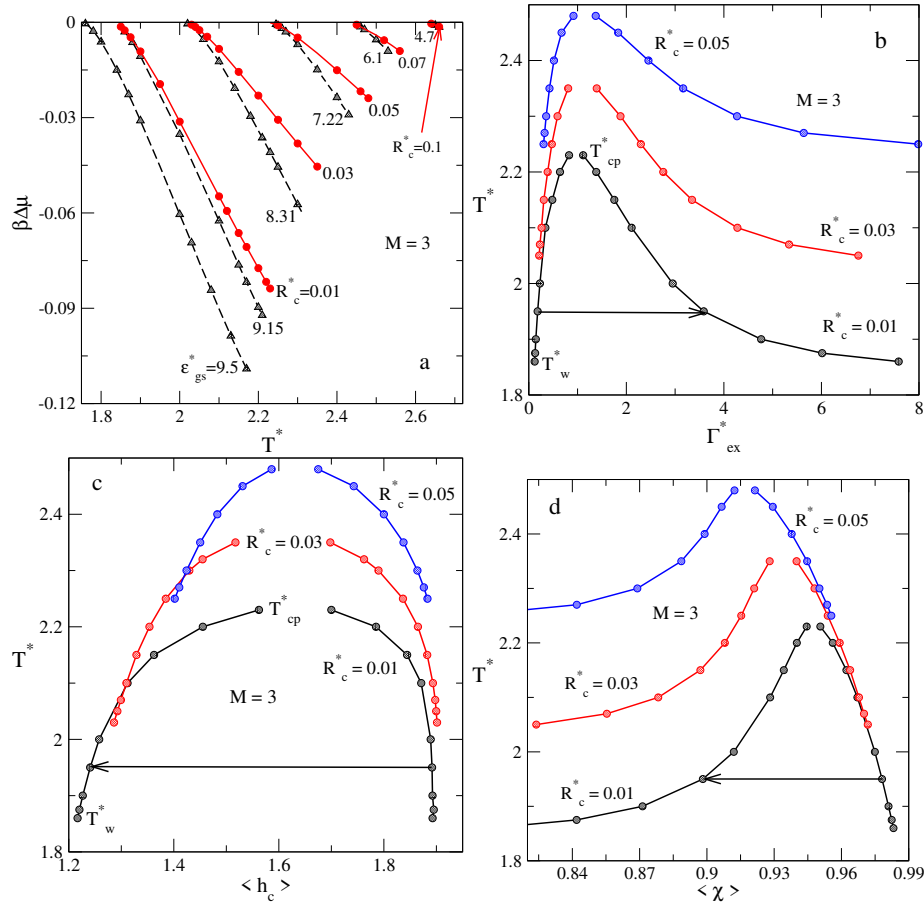


**Figure 3.** (Colour online) Panel a: Prewetting phase diagrams of water on a solid surface with grafted trimers at a different grafting density,  $R_c^* = 0.01, 0.03, 0.05, 0.07$  and  $0.1$  (from left to right - red lines with circles) and on ungrafted substrates with a different adsorbing strength, ( $\epsilon_{gs}^* = 9.5, 9.15, 8.31, 7.22, 6.1$  and  $4.7$ ) — black dashed lines with triangles. Panels b, c and d: The  $T^* - \Gamma_{ex}^*$ ,  $T^* - \langle h_c \rangle$ , and  $T^* - \langle \chi \rangle$  projections of the prewetting phase diagrams, respectively.

Then, we searched for the ungrafted substrates with different  $\epsilon_{gs}^*$  that yield approximately the same  $T_w^*$  for different grafted systems. The entire set of projection in the chemical potential-temperature plane is shown in figure 3a. Illustration of the magnitude of the jump of excess adsorption upon the prewetting transition is given in panel b of figure 3. Each of the envelopes starts below from the wetting temperature,  $T_w^*$ , and ends up at  $T_{cp}^*$ . In contrast to the systems with grafted monomers discussed above, now, for  $M = 3$ , we can construct the panel describing the conformation changes of grafted species upon the prewetting phase transition. This is conveniently given in terms of the jump of the first moment of the density profile of chain species,  $\langle h_c \rangle$ , versus reduced temperature,  $T^*$ , figure 3c. In all cases, we observe that the chains grafted by the first (initial) monomers attain almost a flat configuration on the solid surface upon the formation of a fluid film, as it follows from the  $\langle h_c \rangle$  values after the prewetting transition, figure 3c. Another auxiliary information about the formation of a water film is given in figure 3d. The curves witness the changes of the bonding state of molecules upon the prewetting transition. The branches of the curves to the right of this panel show that the gas-like water vapour contains a high fraction of non-bonded molecules, high values of  $\langle \chi \rangle$ . After the transition, a liquid-like film is formed. The average fraction of non-bonded water molecules is essentially lower in the film, compared to the vapour phase.

The phase diagrams in figure 3 can be illustrated in terms of the microscopic structure. One example of the changes of the density profile of water particles and segments of grafted molecules is presented in figure 4. From figure 4a, we learn that the water film after the prewetting transition is rather dense.

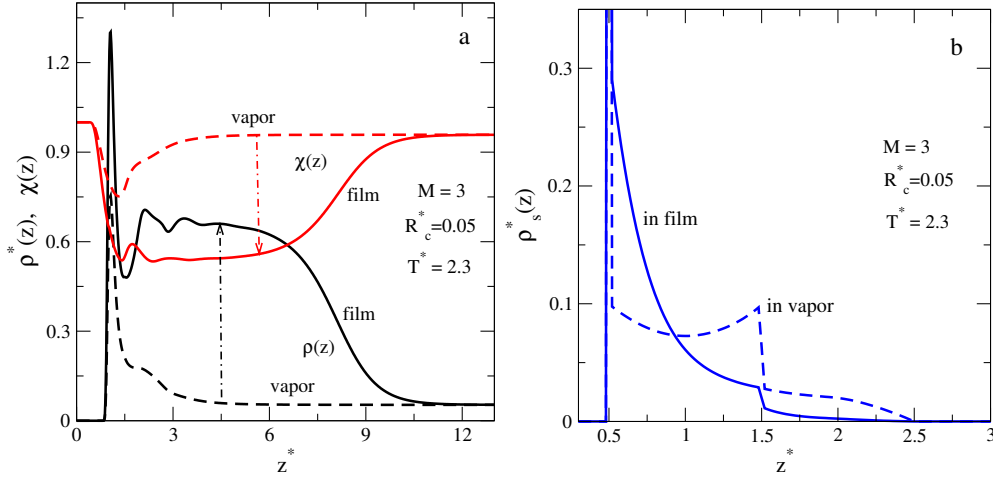


**Figure 4.** (Colour online) Panel a: The density profiles of water species upon the prewetting transition in the system with grafted trimers,  $M = 3$ , at  $R_c^* = 0.05$  and  $T^* = 2.3$  (black lines). The profiles of the fraction of non-bonded molecules before and after transition are shown by red lines. Panel b: Changes of the profile for grafted molecules upon the prewetting transition.

It involves approximately six layers of water molecules whereas the vapor phase before the transition corresponds to a monolayer with a rather small amount of water particles in the second layer. The prewetting transition is accompanied by changes of the fraction of non-bonded species. Vapor phase is mainly composed of non-bonded water molecules. By contrast, the film after transition contains a large amount of molecules that are bonded between themselves. Moreover, the formation of a liquid-like film leads to a drastic change of conformation of grafted trimers. Namely, the segments of trimers are pushed to the surface such that the grafted species attain almost a flat configuration after the transition, figure 4b.

Now, we turn our attention to the effects of attraction between water molecules and segments of grafted trimers. Similarly to the model with grafted monomers, we assume  $\lambda_{fc} = 1.5\sigma$ , and consider apparently modest changes  $\varepsilon_{fc}^*$ , from 0 to 1.5, as in figure 2. A set of results describing the evolution of the prewetting transition lines at different values of the grafting density,  $R_c^*$ , is shown in figure 5a. At a fixed grafting density, the solid surface becomes more attractive upon increasing  $\varepsilon_{fc}^*$  as expected. However, the magnitude of the change of the wetting temperature is different and depends on the value of the grafting density. At higher values of  $R_c^*$ , the changes of wettability are more pronounced. A summarizing insight into the behavior of the wetting temperature and of the prewetting critical temperature with the grafting density is provided in figure 5b. One can see that the substrates with grafted trimers become more hydrophobic upon increasing the grafting density at different values of  $\varepsilon_{fc}^*$  studied. The rate of growth of both characteristic temperatures depends on the assumed value for the energy  $\varepsilon_{fc}^*$ . At the highest value under study,  $\varepsilon_{fc}^* = 1.5$ , the wetting temperature still increases, but very slowly. This behavior is in contrast to the model with grafted monomers, cf. figure 2b. It seems that in the present case one needs to consider even higher values for  $\varepsilon_{fc}^*$  to observe a decreasing wetting temperature. In other words, a stronger affinity between water molecules and segments is needed to cover larger obstacles,  $M = 3$ , to mitigate their blocking capability for adsorption of water, in comparison to the model with  $M = 1$ . Entire picture emerging from the consideration of the systems with grafted trimers and comparison with ungrafted models having approximately the same wetting temperature shows quantitative differences of adsorption of water, especially in the interval of temperatures close to the prewetting critical temperature.

The final stage of our investigation concerns the systems with the grafted pentamers  $M = 5$ . Again, we begin with the case  $\varepsilon_{fc}^* = 0$ . Four panels of figure 6 contain the prewetting phase diagrams of the models with grafted species (panel a), projections describing the changes of excess adsorption (panel b), average height of the grafted layer (panel c) and the average fraction of non-bonded species (panel d) upon the prewetting transition. In addition, we plotted the phase diagrams of the models without grafted pentamers at various  $\varepsilon_{gs}^*$ , that yield similar values for the wetting temperature,  $T_w^*$ . The highest

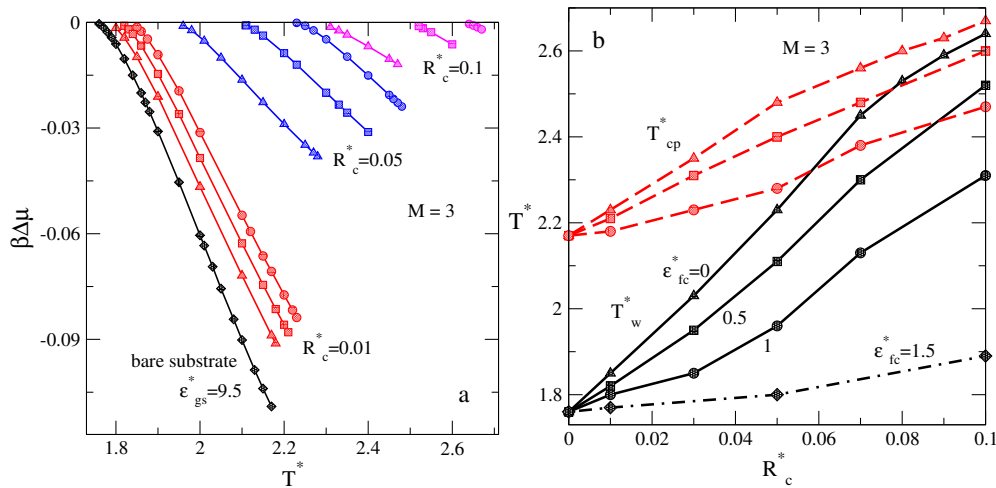


**Figure 5.** (Colour online) Panel a: Prewetting phase diagrams of the system with grafted trimers ( $M = 3$ ) upon the changes of the strength of attraction between the grafted species and water molecules,  $\epsilon_{fc}^* = 0, 0.5$  and  $1$  (lines with circles, squares and triangles, respectively). The red, blue and magenta lines correspond to systems at a different grafting density:  $R_c^* = 0.01, 0.05$  and  $0.1$ , respectively. Panel b: Dependence of the wetting temperature,  $T_w^*$ , and of a prewetting critical temperature,  $T_{cp}^*$ , on the grafted density  $R_c^*$ .

grafting density at which we identified the wetting temperature very close to the bulk critical temperature is  $R_c^* = 0.047$ . The difference between the prewetting transition lines of grafted and ungrafted systems that have a similar wetting temperature is rather big, figure 6a. Besides, the differences between the prewetting critical temperatures are well pronounced. On the other hand, at a fixed temperature, the jump of adsorption upon the prewetting transition in the grafted system ( $R_c^* = 0.02$ ) is larger than in the ungrafted system  $\epsilon_{gs}^* = 7.85$  (both have approximately the same wetting temperature). In addition, the magnitude of change of the average fraction of non-bonded water molecules upon the prewetting transition is more pronounced in the grafted system, figure 6d. It is related to the magnitude of jump of the excess adsorption during transition. The average height of the grafted layer changes as well, figure 6c. If the liquid film is formed, the grafted layer attains the configuration in which segments are between mono- and bilayer.

For illustrative purposes, one example of the changes of the density profiles of water molecules and the total density profile of pentamers upon the prewetting transition is shown in figure 7. The profiles for the fraction of non-bonded water molecules are given in figure 7a as well. Interestingly, the shrinking of the grafted layer of pentamers resembles the trends of behavior of grafted trimers, cf. figure 4b. In the vapor phase, the profiles are different due to the different number of segments. However, after the prewetting transition, pentamers and trimers are pushed into a monolayer type structure, figure 7b.

Similarly to our previous discussion, we now turn our attention to the effects of attraction between water particles and segments of grafted molecules. The width of the square well attractive potential is  $\lambda_{fc} = 1.5\sigma$  as in  $M = 1$  and  $M = 3$  systems. However, the energy of interaction,  $\epsilon_{fc}^*$ , changes. Some examples of the evolution of the prewetting transition lines are given in figure 8a. Apparently, the magnitude of changes of  $T_w^*$  and of  $T_{cp}^*$  depends on  $R_c^*$ , in non-trivial manner. All the models described in this figure exhibit an augmenting wettability, if the attractive interaction between segments of grafted molecules and water becomes stronger. Next, we combined the results for the phase diagrams, at constant  $\epsilon_{fc}^*$ , into the plot illustrating the dependence of characteristic temperatures on the grafting density. These results are shown in figure 8b. The conclusions concerning the behavior of the wetting temperature,  $T_w^*$ , in the systems of grafted pentamers are similar to the trends already observed for grafted trimers,  $M = 3$ , cf. figure 5b. If the attraction between the grafted segments and water molecules is strong enough, e.g.,  $\epsilon_{fc}^* = 1.5$ , the wetting temperature slowly increases upon increasing  $R_c^*$ . If this attraction is weaker, e.g.,  $\epsilon_{fc}^* = 0.5$ , the hydrophobicity of the grafted solid surface grows more rapidly. Apparently, for higher

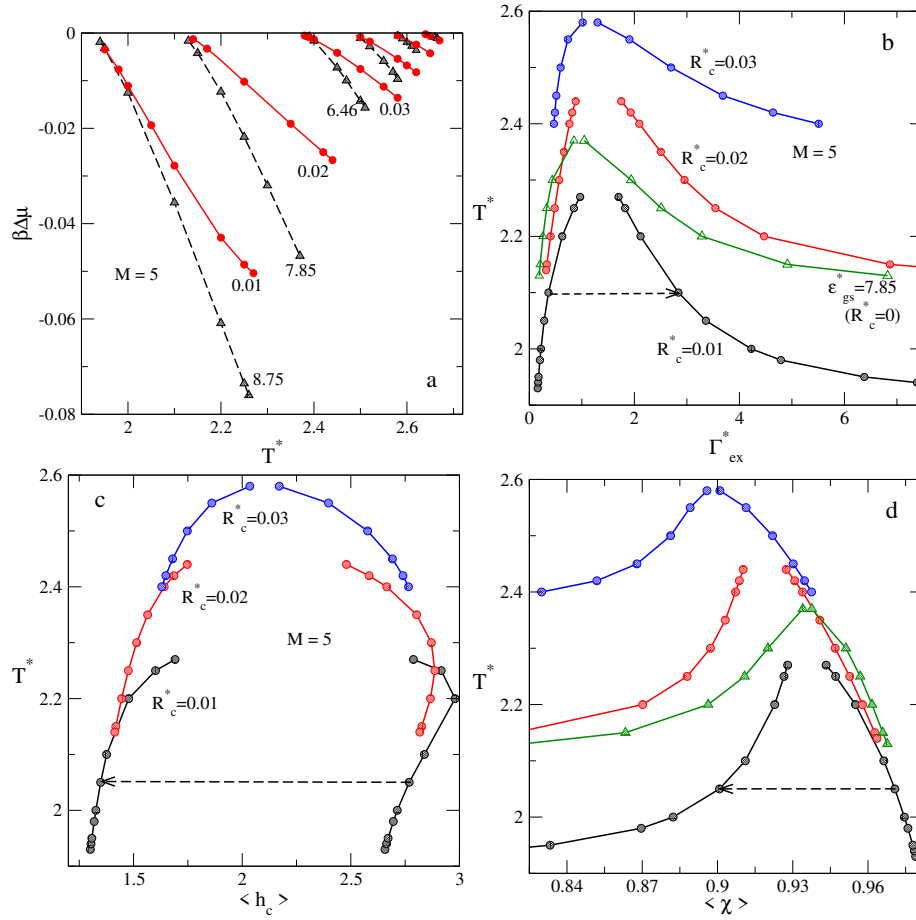


**Figure 6.** (Colour online) Panel a: A comparison of the prewetting phase diagrams for the systems with the grafted pentamers,  $M = 5$ , at  $R_c^* = 0.01, 0.02, 0.03, 0.035, 0.04$  and  $0.045$  (red lines with triangles) and for bare substrates with different adsorbing strength,  $\epsilon_{gs}^*$ , black lines with circles, at 8.75, 7.85, 6.46, 5.83, 5.23 and 4.6. Some of these numbers are indicated in the figure for a better identification of the curves. Panels b, c and d: The  $T^* - \Gamma_{ex}^*$ ,  $T^* - \langle h_c \rangle$ , and  $T^* - \langle \chi \rangle$  projections of the prewetting phase diagrams, respectively. The phase diagram projections for an ungrafted substrate with  $\epsilon_{gs}^* = 7.85$  are shown in panels b and d for comparison. The nomenclature of colors is the same in panels b and d.

values of the parameter  $\epsilon_{fc}^*$ , one may observe the curve with decreasing values for  $T_w^*$  upon increasing grafted density  $R_c^*$ . At present, we obtained a wavy behavior for the prewetting critical temperature,  $T_{cp}^*$ , with increasing  $R_c^*$  at a moderate attraction strength between segments and water molecules (cf. figure 8 of [29] for the behavior of the wetting temperature on the grafting density of monomers from the evaluation of contact angles).

## 5. Summary and conclusions

We have studied the problem of wetting a solid surface chemically modified by grafted short chain molecules by water using a simple model that well captures the bulk phase behavior and applies 10-4-3 interaction potential for water-graphite-type solid interaction. The chain molecules are modelled as tangentially bonded hard sphere segments that may interact with water as well. The theory is a version of the classical density functional approach. Our principal focus is on the determination of the wetting temperature and the construction of the prewetting phase diagrams. The fluid chemical potential-temperature projection of the phase diagram is evaluated for several grafted systems with monomers,

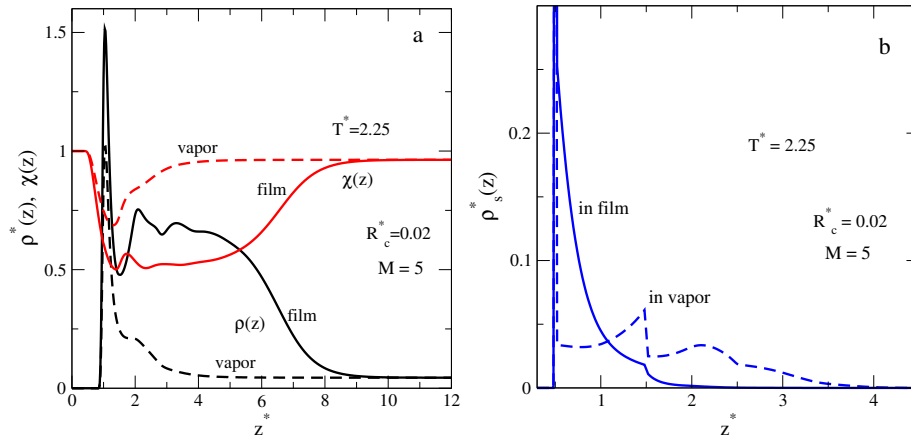


**Figure 7.** (Colour online) Panel a: The density profiles of water species upon the prewetting transition in the system with grafted pentamers,  $M = 5$ , at  $R_c^* = 0.02$  and  $T^* = 2.25$  (black lines). The profiles for the fraction of non-bonded molecules before and after transition are shown by red lines. Panel b: Changes of the profile for grafted molecules upon the prewetting transition.

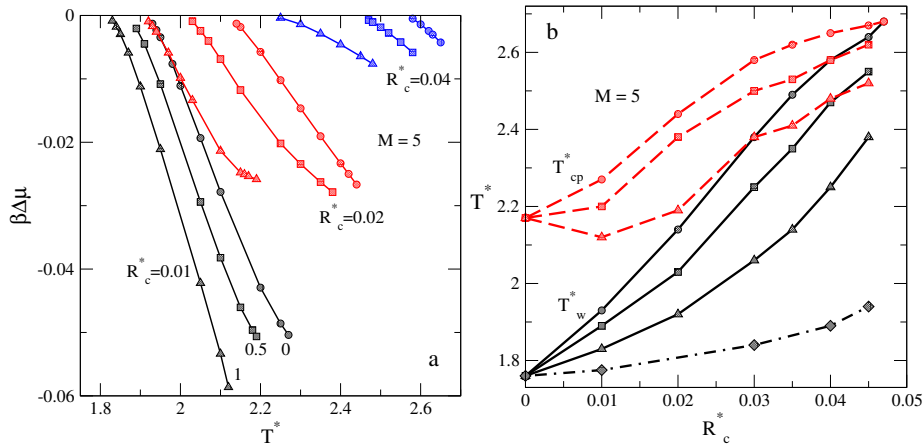


**Figure 8.** (Colour online) Panel a: Prewetting phase diagrams of the system with grafted pentamers ( $M = 5$ ) upon changes of the strength of attraction between grafted species and water molecules,  $\varepsilon_{fc}^* = 0, 0.5$  and  $1$  (lines with circles, squares and triangles, respectively). The black, red and blue lines correspond to systems at a different grafting density:  $R_c^* = 0.01, 0.02$  and  $0.04$ , respectively. Panel b: Evolution of the wetting temperature,  $T_w^*$  (black lines), and of the prewetting critical temperature,  $T_{cp}^*$  (red lines), with grafted density  $R_c^*$ . The lines decorated with circles, squares and triangles correspond to  $\varepsilon_{fc}^* = 0, 0.5$  and  $1$ , respectively. The line with diamonds is for  $\varepsilon_{fc}^* = 1.5$ .

trimers and pentamers as the grafted species. A detailed comparison is performed with the wetting behavior of water on differently adsorbing bare graphite-like surfaces. It is described how the presence of grafted chains modify the prewetting transition line. Other projections for the prewetting transition on temperature, grafting density, the number of segments and on the attraction strength between segments of grafted species and water molecules are obtained and analyzed. Surface thermodynamic results are illustrated by the fluid density profiles and the total segment density profiles in some cases. All the results are consistent and physically reasonable. At the moment, we are not able to confront our findings with experimental data. Probably, the models in question are too simple and need to include various elements to make them closer to the laboratory setup. Nevertheless, the present study can be supplemented by the calculations of the temperature trends of the contact angle to make a link with the data for water on

heterogeneous surfaces. For some systems that involve simple fluids in contact with solids, studied so far, predictions of the density functional theory are confirmed by computer simulations. We expect that similar developments will be performed concerning the phenomena studied in the present work.

The models of the present investigation permit and require various important extensions. Undoubtedly, for future studies of selective adsorption one needs to modify our numerical software to mixtures of water with either organic co-solvent or solutions of interest in various applications. Methodologically, it is important to include the effects of chemical association between most exposed, terminating segment of grafted species with fluid particles. On the other hand, it is of interest to include more sophisticated interactions between segments belonging to different grafted molecules. The effects of stiffness of grafted chain species are worth taking into account as well. Some of these problems are under study in our laboratory. These elements, precisely, would contribute to making the present primitive model smarter and more suitable to find laboratory-type applications.

## Acknowledgements

Author acknowledges helpful discussions with Prof. Myroslav Holovko. Technical support of Magdalena Aguilar at the Institute of Chemistry of the UNAM is gratefully acknowledged. Support by CONAHcyT of Mexico under the grant CBF2023-2024-2725 is acknowledged as well.

## References

1. Yukhnovskii I. R., Rakhimova I. S., Vladimirov V. V., *Ukr. Fiz. Zh.*, 1959, 4, 334, (in Ukrainian).
2. Percus J. K., Yeveick G. J., *Phys. Rev.*, 1957, **110**, 1, doi:10.1103/PhysRev.110.1.
3. Henderson D., Abraham F. F., Barker J. A., *Mol. Phys.*, 1976, **31**, 1291, doi:10.1080/00268977600101021.
4. Blum L., *J. Phys. Chem.*, 1977, **81**, 136, doi:10.1021/j100517a009.
5. Henderson D., Blum L., *J. Chem. Phys.*, 1978, **69**, 5441, doi:10.1063/1.436535.
6. Yukhnovskii I. R., Kuryliak I. I., *Ukr. Fiz. Zh.*, 1976, 21, 1772, (in Ukrainian).
7. Kurylyak I. I., Yukhnovskii I. R., *Theor. Math. Phys.*, 1982, 52, No. 1, 691–699, doi:10.1007/BF01027790.
8. Yukhnovskii I. R., Holovko M. F., Kuryliak I. I., Soviak E. M. In: *Fizika molekul*, Vol. 10, Naukova dumka, Kiev, 1981, 26–43, (in Russian).
9. Yukhnovskii I. R., Holovko M. F., Soviak E. N., Preprint of *Inst. Theor. Phys. Ukr. Acad. Sci.*, ITP-82-159R, Kiev, 1982, (in Russian).
10. Golovko M. F., Blotsky S. N., Pizio O., *Electrochim. Acta*, 1989, **34**, 63, doi:10.1016/0013-4686(89)80010-6.
11. Yukhnovskyi I. R., Holovko M. F., *Statistical Theory of Classical Equilibrium Systems*, Naukova dumka, Kyiv, 1980, (in Russian).
12. Golovko M. F., Yukhnovskii I. R., *Approaches to the Many-Body Theory of Dense Ion-Dipole Plasma. Application to Ionic Solvation*. In: *The Chemical Physics of Solvation*, Vol. A. Elsevier, Amsterdam, 1985, 207–262.
13. Holovko M. F., Kuryliak I. I., Pizio O. A., Sovjak E. N., In: *Problems of Contemporary Statistical Physics*, N. N. Bogololiubov (Ed.), Naukova Dumka Publishers, Kyiv, 1985, 82–96, (in Russian).
14. Holovko M. F., Vakarin E. V., *Mol. Phys.*, 1995, **84**, 1057, doi:10.1080/00268979500100741.
15. Holovko M. F., Vakarin E. V., Duda Yu.Ya., *Chem. Phys. Lett.*, 1995, **233**, 420, doi:10.1016/0009-2614(94)01480-J.
16. Pizio O., Henderson D., Sokolowski S., *J. Phys. Chem.*, 1995, **99**, 2408, doi:10.1021/j100008a025.
17. Patrykiewicz A., Sokolowski S., Pizio O., In: *Surface and Interface Science*, Wandelt K. (Ed.), Wiley, 2016, 883–1253, doi:10.1002/9783527680580.ch46.
18. Patsahan O. V., Mryglod I. M., *Condens. Matter Phys.*, 2012, **15**, 24001, doi:10.5488/CMP.15.24001.
19. Huerta A., Pizio O., Bryk P., Sokolowski S., *Mol. Phys.*, 2000, **98**, 1851, doi:10.1080/00268970009483390.
20. Millan Malo B., Pizio O., Patrykiewicz A., Sokolowski S., *J. Phys.: Condens. Matter*, 2001, **13**, 1361, doi:10.1088/0953-8984/13/7/303.
21. Millan Malo B., Salazar L., Sokolowski S., Pizio O., *J. Phys.: Condens. Matter*, 2000, **12**, 8785, doi:10.1088/0953-8984/12/41/304.
22. Patrykiewicz A., Sokolowski S., Sokolowska Z., Pizio O. *J. Phys.: Condens. Matter*, 2001, **13**, 6151, doi:10.1088/0953-8984/13/28/301.
23. Clark G. N., Haslam A. J., Galindo A., Jackson G., *Mol. Phys.*, 2006, **104**, 3561, doi:10.1080/00268970601081475.

24. Trejos V. M., Pizio O., Sokolowski S., *Fluid Phase Equilib.*, 2018, **473**, 145, doi:10.1016/j.fluid.2018.06.005.
25. Trejos V. M., Pizio O., Sokolowski S., *J. Chem. Phys.*, 2018, **149**, 134701, doi:10.1063/1.5066552.
26. Pizio O., Sokolowski S., *Mol. Phys.*, 2022, **120**, e2011454, doi:10.1080/00268976.2021.2011454.
27. Pizio O., Sokolowski S., *J. Mol. Liq.*, 2022, **357**, 119111, doi:10.1016/j.molliq.2022.119111.
28. Pizio O., Sokolowski S., *J. Mol. Liq.*, 2023, **390**, 123009, doi:10.1016/j.molliq.2023.123009.
29. Dabrowska K., Pizio O., Sokolowski S., *Condens. Matter Phys.*, 2022, **25**, 33603, doi:10.5488/CMP.25.33603.
30. Pizio O., Patrykiewicz A., Vega C., Pusztai L., Ilnytskyi J., Patsahan T., Trokhymchuk A., *Condens. Matter Phys.*, 2024, **27**, 37001, doi:10.5488/CMP.27.37001.
31. Brittain W. J., Minko S., *J. Polym. Sci., Part A: Polym. Chem.*, 2007, **45**, 3505, doi:10.1002/pola.22180.
32. Stockhausen V., Trippé-Allard G., Van Quynh N., Ghilane J., Lacroix J.-C., *J. Phys. Chem. C*, 2015, **119**, 19218, doi:10.1021/acs.jpcc.5b05456.
33. Gutiérrez Morenó J. J., Pan K., Wang Y., Li W., *Langmuir*, 2020, **36**, 5680, doi:10.1021/acs.langmuir.9b03755.
34. Obeso J. L., Lopez Cervantes V. B., Flores C. V., Garcia-Carvajal C., Garduño-Albino C. E., Peralta R. A., Trejos V. M., Arcos L. H., Ibarra I. A., Solis-Ibarra D., Cordero-Sánchez S., Portillo-Vélez N. S., Esparza-Schulz J. M., *Dalton Trans.*, 2024, **53**, 12208, doi:10.1039/d4dt01283f.
35. Halperin A., de Gennes P. G., *J. Phys. (Paris)*, 1986, **47**, 1243, doi:10.1051/jphys:019860047070124300.
36. Bryuzgin E. V., Hyakutake T., Navrotsky A. V., Nishide H., Novakov I. A., *Prot. Met. Phys. Chem. Surf.*, 2013, **49**, 101, doi:10.1134/S207020511301005X.
37. Long D., Ajdari A., Leibler L., *Langmuir*, 1996, **12**, 1675, doi:10.1021/la950701n.
38. Rutledge J. E., Taborek P., *Phys. Rev. Lett.*, 1992, **69**, 937, doi:10.1103/PhysRevLett.69.937.
39. Xu X., Cao D., *J. Chem. Phys.*, 2009, **130**, 164901, doi:10.1063/1.3119311.
40. Haghmoradi A., Wang L., Chapman W. G., *J. Phys.: Condens. Matter*, 2017, **29**, 044002, doi:10.1088/1361-648x/29/4/044002.
41. Bryk P., MacDowell L. G., *J. Chem. Phys.*, 2011, **135**, 204901, doi:10.1063/1.3662139.
42. Chen C., Tang P., Qiu F., Shi A.-C., *J. Chem. Phys.*, 2011, **135**, 204901, doi:10.1063/1.4916133.
43. Jain S., Jog P., Weinhold J., Srivastava R., Chapman W. G., *J. Chem. Phys.*, 2008, **128**, 154910, doi:10.1063/1.2902976.
44. Li C., Zhang T., Yang Y., Tang P., *ACS Omega*, 2019, **4**, 12927, doi:10.1021/acsomega.9b01800.
45. Yu Y.-X., Wu J., *J. Chem. Phys.*, 2002, **117**, 2368, doi:10.1063/1.1491240.
46. Patrykiewicz A., Sokolowski S., Tscheliessnig R., Fischer J., Pizio O., *J. Phys. Chem. B*, 2008, **112**, 4552, doi:10.1021/jp710978t.
47. Kozina A., Aguilar A., Pizio O., Sokolowski S., *Condens. Matter Phys.*, 2024, **27**, 13604, doi:10.5488/CMP.27.13604.
48. Trejos V. M., Pizio O., Sokolowski S., *J. Chem. Phys.*, 2018, **149**, 234703, doi:10.1063/1.5066552.
49. Trejos V. M., Pizio O., Sokolowski S., *J. Chem. Phys.*, 2019, **151**, 064704, doi:10.1063/1.5116128.
50. Müller E. A., Gubbins K. E., *Ind. Eng. Chem. Res.*, 2011, **40**, 2193, doi:10.1021/ie000773w.
51. Steele W. A., *The Interaction of Gases with Solid Surfaces*, Pergamon Press, Oxford, 1974.
52. Friedman S. R., Khalil M., Taborek P., *Phys. Rev. Lett.*, 2013, **111**, 226101, doi:10.1103/PhysRevLett.111.226101.
53. Gatica S. M., Johnson J. K., Zhao X. C., Cole M. W., *J. Phys. Chem. B*, 2004, **108**, 11704, doi:10.1021/jp048509u.
54. Dutta R. C., Khan S., Singh V., *Fluid Phase Equilib.*, 2011, **302**, 310, doi:10.1016/j.fluid.2010.07.006.
55. Fletcher D. A., McMeeking R. F., Parkin D., *J. Chem. Inf. Comput. Sci.*, 1996, **36**, No. 4, 746–749, doi:10.1021/ci960015+.
56. Zhao X., *Phys. Rev. B*, 2007, **76**, 041402(R), doi:10.1103/PhysRevB.76.041402.
57. Pizio O., Pusztai L., Sokolowska Z., Sokolowski S., *J. Chem. Phys.*, 2009, **130**, 134501, doi:10.1063/1.3103266.
58. Sokolowski S., Ilnytskyi J., Pizio O., *Condens. Matter Phys.*, 2014, **17**, 12601, doi:10.5488/CMP.17.12601.
59. Jackson G., Chapman W. G., Gubbins K. E., *Mol. Phys.*, 1988, **65**, 1, doi:10.1080/00268978800100821.
60. Chapman W. G., Jackson G., Gubbins K. E., *Mol. Phys.*, 1988, **65**, 1057, doi:10.1080/00268978800101601.
61. Yu Y.-X., Wu J., *J. Chem. Phys.*, 2002, **117**, 10156, doi:10.1063/1.1520530.
62. Kreer T., Metzger S., Müller M., Binder K., Baschnagel J., *J. Chem. Phys.*, 2004, **120**, 4012, doi:10.1063/1.1642615.
63. Dimitrov D., Milchev A., Binder K., *Macromol. Symp.*, 2007, **252**, 47, doi:10.1002/masy.200750605.

## До побудови мікроскопічної моделі для смарт-покриття твердої поверхні

О. Пізіо

Інститут хімії, Національний автономний університет Мексики, Сіркуіто Екстеріор, 04510 Мехіко, Мексика

Підхід функціоналу густини для класичних асоціативних рідин використовується для дослідження фазових діаграм змочування для модельних систем, що складаються з води та графітоподібних твердих поверхонь, хімічно модифікованих невеликою кількістю приєднаних ланцюгових молекул. Модель водоподібної рідини запозичено з роботи Кларка та ін. [Mol. Phys., **104**, 3561 (2006)]. Вона дуже добре описує співіснування води та пари в об'ємі. Кожна ланцюгова молекула складається з тангенціально зв'язаних сегментів твердих сфер. Ми зосереджуємося на дослідженні росту водяної плівки на таких складних підкладках та вивченні поведінки змочування. Для приєднаних мономерів фазові діаграми попереднього змочування подібні до діаграм для води на немодифікованій твердій поверхні. Однак для приєднаних тримерів і пентамерів спостерігається та аналізується набагато цікавіша фізична поведінка. Детально обговорюються тенденції залежностей температури змочування та критичної температури попереднього змочування від густини приєднаних частинок та притягання комплексів води.

**Ключові слова:** *теорія функціоналу густини, модель води, профілі густини, адсорбція, температура змочування*

---

---